# An adaptive numerical strategy for the medium-frequency analysis of Helmholtz's problem

Hervé Riou, Pierre Ladevèze, Benjamin Sourcis, Béatrice Faverjon, Louis Kovalevsky

# AN ADAPTIVE NUMERICAL STRATEGY FOR THE MEDIUM-FREQUENCY ANALYSIS OF HELMHOLTZ'S PROBLEM

HERVÉ RIOU*, PIERRE LADEVÈZE† and BENJAMIN SOURCIS‡

*LMT-Cachan (ENS Cachan/CNRS/Univ. Paris 6, PRES UniverSud Paris)*
*61 avenue du Président Wilson, F-94230 Cachan, France*
**riou@lmt.ens-cachan.fr*
†*ladeveze@lmt.ens-cachan.fr*
‡*sourcis@lmt.ens-cachan.fr*

BÉATRICE FAVERJON

*LaMCoS/DCS — INSA de Lyon Batiment Jean D'Alembert*
*18-20, rue des Sciences, F69621 Villeurbanne Cedex, France*
*Beatrice.Faverjon@insa-lyon.fr*

LOUIS KOVALEVSKY

*LMT-Cachan (ENS Cachan/CNRS/Univ. Paris 6, PRES UniverSud Paris)*
*61 avenue du Président Wilson, F-94230 Cachan, France*
*kovalevsky@lmt.ens-cachan.fr*

The variational theory of complex rays (VTCR) is a wave-based predictive numerical tool for medium-frequency problems. In order to describe the dynamic field variables within the substructures, this approach uses wave shape functions which are exact solutions of the governing differential equation. The discretized parameters are the number of substructures ($h$) and the number of wavebands ($p$) which describe the amplitude portraits. Its capability to produce an accurate solution with only a few degrees of freedom and the absence of pollution error make the VTCR a suitable numerical strategy for the analysis of vibration problems in the medium-frequency range. This approach has been developed for structural and acoustic vibration problems. In this paper, an error indicator which characterizes the accuracy of the solution is introduced and is used to define an adaptive version of the VTCR. Numerical illustrations are given.

*Keywords*: Medium-frequency; Helmholtz equation; acoustics; adaptive numerical strategy; variational theory of complex rays.

## 1. Introduction

In recent years, the study of the vibrational behavior of mechanical systems has become a cornerstone of the design of industrial products and of the optimization of their performances. In the automotive industry, for instance, vehicle bodies have become thinner and thinner and, therefore, more prone to vibrations. Aerospace structures have become lighter and lighter, giving the study of vibrations a major role in design processes. The cost of experimental tests and the growing demand for prediction tools have made Computer Aided Engineering (CAE) tools essential. Today, the finite element method (FEM)[1] and the boundary element method (BEM)[2] are the CAE tools of reference for the analysis of vibration problems.

The FEM consists in using a large (but finite) number of small elements to discretize the problem. The dynamic field variables are described in terms of polynomial shape functions. However, since these shape functions are not exact solutions of the governing differential equations, a refined discretization is required in order to eliminate the associated pollution error[3] and achieve reasonable prediction accuracy at higher frequencies. This results in large numerical models whose resolution requires prohibitively large computational resources. As a result, the FEM is limited to low-frequency applications.[4] A variety of techniques have been proposed in order to circumvent these problems, including modifications of the standard finite element method such as predefined reduced bases,[5] the Galerkin least-squares FEM,[6] the quasi-stabilized finite element method,[7] the partition of unity method (PUM),[8,9] the generalized finite element method,[10] and residual-free bubbles.[11,12] Compared to standard finite elements, these techniques have been shown to reduce computational costs. However, the frequency ranges which they are capable of addressing are still lower than what would be desirable.

The BEM is based on a boundary integral formulation of the problem, so only the boundary of the domain being considered needs to be discretized. Within the boundary elements which constitute the model, some boundary variables are expressed in terms of simple polynomial shape functions. Compared to FE models, the application of the boundary conditions results in a small system of equations to be solved for the nodal values at the discretized boundary. Once these nodal values have been determined, the field variables inside the domain can be reconstructed in a postprocessing step using the boundary integration formulation. Since the boundary alone has to be discretized, the BEM is exempt from some of the problems mentioned concerning the FEM. However, even though some improvements have been made to the BEM in order to increase its efficiency,[13,14] the construction of the frequency-dependent and fully populated matrices is very time consuming. Moreover, the integration of singular Green functions is the source of numerical difficulties.[15,16]

Today, there are also dedicated computational strategies for the resolution of medium-frequency problems, known as Trefftz methods,[17] which differ from the FEM and the BEM in that in many cases the shape functions are exact solutions of the governing differential equations. These approaches include, for example, a special use of the PUM,[18–20] the ultra-weak variational method,[21] the least-squares method,[22] the discontinuous enrichment method

(DEM),[23] the element-free Galerkin method,[24] the wave boundary element method,[25] and the wave-based method.[26] All these numerical techniques use oscillating functions to solve the problem. The main differences concern the treatment of the transmission conditions between substructures and the boundary conditions. The variational theory of complex rays (VTCR), which is the subject of this paper, belongs to that category.

The VTCR was proposed in Refs. 27 and 28 for the resolution of vibration problems in the medium-frequency range. It is based on an original variational formulation of the problem which was developed in order to enable approximations within subdomains to be *a priori* independent of one another. In each subdomain, any type of shape function can be used, which brings this approach great flexibility and robustness. For vibration problems, the VTCR approximates the solution through a set of wave functions, called complex rays, which verify the governing differential equations exactly. Therefore, no residual error affects the governing partial differential equations inside the subdomains. However, the functions may violate the boundary conditions. Setting the residual boundary errors to zero using the previous variational formulation leads to a small matrix equation whose solution gives the angular distribution of the waves in space. In Ref. 29, the VTCR was used to predict the vibrational response of a 3D plate assembly. In Ref. 30, plates with heterogeneities were taken into account. In Ref. 31, that theory was extended to shell structures. The calculation of the vibrational response over a range of frequencies was presented in Ref. 32. The use of the VTCR for transient dynamic problems was addressed in Ref. 33. Finally, the extension to acoustic problems was presented in Ref. 34. Many examples have shown that this approach is capable of producing an accurate solution using only a small number of degrees of freedom (DOFs).

This paper shows how the efficiency of the VTCR for the study of interior acoustic problems governed by a Helmholtz-type partial differential equation can be improved. A first error indicator for controlling the calculation is derived based on the residuals of the boundary conditions calculated in a subcavity. Using this error indicator, an adaptive version of the VTCR is formulated. The adaptive nature of this new version is interesting in some cases where the directions of propagation of the waves are not distributed uniformly in space. Indeed, there are structures in which the boundaries guide the waves along specific directions, in which case there is no need for the waves to be densely distributed in all spatial directions. The VTCR is very well-suited for such anisotropic discretizations and the proposed error indicator enables one to determine whether a refined angular discretization of the waves is necessary or not. Based on these considerations, the adaptive VTCR works as follows: A first calculation is performed using a coarse angular wave discretization; next, a second calculation is carried out in order to evaluate the need for a refined mesh in each angular direction; a third and final calculation is then carried out with a mixed coarse and refined angular discretization. A new error calculation is performed, and the refinement process can start again.

The paper is organized as follows: Sec. 2 briefly describes the general vibration problem to be solved and the VTCR approach. Section 3 presents the error indicator for the VTCR. Section 4 describes the adaptive version of the VTCR. Section 5 shows numerical examples

of applications of the method. Finally, Sec. 6 concludes the paper with general remarks and proposes some perspectives for future research.

## 2. The Variational Theory of Complex Rays for Helmholtz Problems

This section reviews the basic principles of the VTCR modeling methodology for the resolution of Helmholtz's equation (for more details, see Ref. 27). First, the general problem to be solved is defined. Then, the different steps of the VTCR computational approach are presented in detail.

### 2.1. *The reference problem*

For the sake of simplicity, let us consider a general two-dimensional steady-state interior dynamic problem in an acoustic cavity $\Omega$ divided into two subcavities $\Omega_1$ and $\Omega_2$ with an interface $\Gamma$ (see Fig. 1).

The cavity $\Omega$ is filled with an incompressible fluid characterized by its sound velocity $c_0$ and its density $\rho_0$. The steady-state dynamic behavior of $\Omega$ is studied at a fixed circular frequency $\omega$. All the descriptive quantities can be expressed as complex numbers: An amplitude $Q(\mathbf{x})$ is associated with the quantity $Q(\mathbf{x})e^{i\omega t}$, where $\mathbf{x}$ represents the position and $i = \sqrt{-1}$ the imaginary unit.

Each subcavity $\Omega_E (E \in \{1, 2\})$ is subjected to excitations applied along $\partial\Omega_E = \partial_p\Omega_E \cup \partial_v\Omega_E \cup \partial_Z\Omega_E \cup \Gamma$ in the form of a prescribed pressure $p_{dE}$ over $\partial_p\Omega_E$, a prescribed normal velocity $v_{dE}$ over $\partial_v\Omega_E$, a mixed excitation over $\partial_Z\Omega_E$ and the conditions imposed by the other subcavities. The mixed condition applied to part $\partial_Z\Omega_E$ of $\partial\Omega_E$, called a Robin condition, introduces absorption through its real part. Let us define operator $L_v[\square_E]$ as

$$L_v[\square_E] = \frac{i}{\rho_0\omega}\frac{\partial\square_E}{\partial\mathbf{n}_E} = \frac{i}{\rho_0\omega}\mathbf{n}_E^T.\nabla(\square_E), \tag{1}$$

where $\mathbf{n}$ is the outward normal to $\Omega_E$.

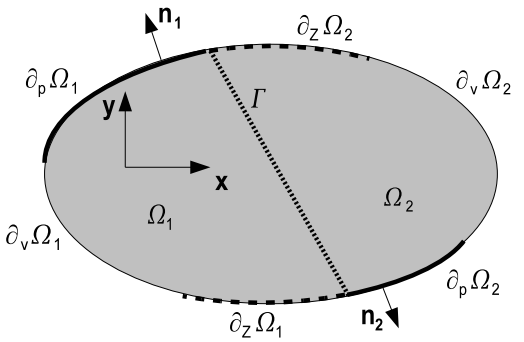


Fig. 1. A general 2D bounded Helmholtz problem.

The reference problem to be solved consists in finding the acoustic pressure $(p_1, p_2) \in H^1(\Omega_1) \times H^1(\Omega_2)$ such that

$$\Delta p_E + k^2 p_E = 0 \in \Omega_E, E \in \{1, 2\}, \tag{2}$$

$$\left| \begin{array}{lll} p_E = p_{dE} & \text{over} & \partial_p \Omega_E \\ L_v[p_E] = v_{dE} & \text{over} & \partial_v \Omega_E, \quad E \in \{1, 2\} \\ p_E - Z_E L_v[p_E] = h_{dE} & \text{over} & \partial_Z \Omega_E \end{array} \right. , \tag{3}$$

$$\left| \begin{array}{lll} p_1 - p_2 = 0 & \text{over} & \Gamma \\ L_v[p_1] + L_v[p_2] = 0 & \text{over} & \Gamma. \end{array} \right. \tag{4}$$

Equation (2) is the homogeneous Helmholtz equation, with $k = \omega/c_0$ being the wave number. Equations (3) and (4) are related to the boundary conditions of the problem and the continuity conditions at the interface between the two subcavities $\Omega_1$ and $\Omega_2$. $Z_E$ is an impedance coefficient.

### 2.2. *Variational formulation of the problem*

A weak form of the reference problem introduced in Sec. 2.1 can be derived using a variational formulation introduced in Ref. 27. This formulation uses power quantities and verifies the boundary conditions (3) and (4) in a weak sense. Thus, the resulting approximation includes exact solutions of the Helmholtz equation (2).

Let $S_{ad}^E$ denote the space of the functions which verify Helmholtz's homogeneous equation (2) throughout cavity $\Omega_E$:

$$S_{ad}^E = \{p_E \in H^1(\Omega_E) \,|\, \Delta p_E + k^2 p_E = 0, \forall \mathbf{x} \in \Omega_E\}. \tag{5}$$

The partial differential equation problem defined by (2), (3) and (4) can be expressed as follows:

Find $(p_1, p_2) \in S_{ad}^1 \times S_{ad}^2$ such that

$$\begin{aligned} \mathrm{Re}\Bigg\{ & \sum_{E=1,2} \int_{\partial_p \Omega_E} (p_E - p_{dE}) \cdot \overline{L_v[\delta p_E]} ds + \sum_{E=1,2} \int_{\partial_v \Omega_E} \overline{(L_v[p_E] - v_{dE})} \cdot \delta p_E ds \\ & + \frac{1}{2} \sum_{E=1,2} \int_{\partial_Z \Omega_E} (((1 - Z_E L_v)[p_E] - h_{dE}) \cdot \overline{L_v(\delta p_E)} \\ & + (\overline{(L_v - 1/Z_E)[p_E] + h_{dE}/Z_E)} \cdot \delta p_E) ds + \frac{1}{2} \int_\Gamma ((p_1 - p_2) \cdot \overline{L_v[\delta p_1 - \delta p_2]} \\ & + \overline{L_v[p_1 + p_2]} \cdot (\delta p_1 + \delta p_2)) ds \Bigg\} = 0, \quad \forall (\delta p_1, \delta p_2) \in S_{ad}^1 \times S_{ad}^2, \end{aligned} \tag{6}$$

where $\overline{\square}$ and $\mathrm{Re}\{\square\}$ designate respectively the complex conjugate and the real part of the complex quantity $\square$. The generalization of this variational formulation to an assembly of $n$ subcavities is straightforward.

This formulation can be viewed as the expression of a power balance at each boundary of the subcavities $\Omega_E$. This is a mixed asymmetrical formulation which enables the approximations in the subcavities to be independent of one another. This property grants the strategy great flexibility and efficiency because no Lagrange multiplier or penalty term is necessary in order to ensure interelement continuity.

Since (6) is not a classical variational formulation, proof of the equivalence with reference problem (2), (3), (4), whose solution clearly satisfies (6), must be given. In order to do that, let us consider two solutions $(p_1, p_2)$ and $(p_1', p_2')$ of the variational formulation and let $\tilde{p} = (\tilde{p}_1, \tilde{p}_2)$ denote the differences between the two. Because of (6), these two solutions must verify the following equation:

$$\begin{aligned}\mathrm{Re}\Bigg\{ &\sum_{E=1,2} \frac{1}{2}\int_{\partial_p\Omega_E} (\tilde{p}_E)\cdot\overline{L_v[\delta p_E]}ds + \sum_{E=1,2}\int_{\partial_v\Omega_E}\overline{L_v[\tilde{p}_E]}\delta p_E ds \\ &+ \sum_{E=1,2}\frac{1}{2}\int_{\partial_Z\Omega_E}(((1-Z_EL_v)[\tilde{p}_E])\cdot\overline{L_v(\delta p_E)} + (\overline{(L_v - 1/Z_E)[\tilde{p}_E]})\cdot\delta p_E)\,ds \\ &+ \frac{1}{2}\int_\Gamma((\tilde{p}_1-\tilde{p}_2)\cdot\overline{L_v[\delta p_1 - \delta p_2]} + \overline{L_v[\tilde{p}_1+\tilde{p}_2]}\cdot(\delta p_1 + \delta p_2))\,ds\Bigg\} = 0. \end{aligned} \tag{7}$$

Taking $\delta p = \tilde{p}$, (7) simplifies trivially to:

$$\begin{aligned} a(\tilde{p},\tilde{p}) = \mathrm{Re}\Bigg\{ &\sum_{E=1,2}\oint_{\partial\Omega_E}\tilde{p}_E\overline{L_v[\tilde{p}_E]}ds \\ &- \sum_{E=1,2}\frac{1}{2}\int_{\partial_Z\Omega_E}\left(Z_EL_v[\tilde{p}_E]\overline{L_v[\tilde{p}_E]} + \frac{1}{Z_E}\tilde{p_E}\overline{\tilde{p}_E}\right)ds\Bigg\} = 0. \end{aligned} \tag{8}$$

The Strokes formula applied to each subcavity $\Omega_E$ yields:

$$\begin{aligned} a(\tilde{p},\tilde{p}) = \mathrm{Re}\Bigg\{ &\sum_{E=1,2} -\frac{i}{\rho_0\omega}\int_{\Omega_E}(\nabla\tilde{p}_E\cdot\overline{\nabla\tilde{p}_E} + \tilde{p}_E\Delta\overline{\tilde{p}_E})\,d\Omega \\ &- \sum_{E=1,2}\frac{1}{2}\int_{\partial_Z\Omega_E}\left(Z_EL_v[\tilde{p}_E]\overline{L_v[\tilde{p}_E]} + \frac{1}{Z_E}\tilde{p_E}\overline{\tilde{p}_E}\right)ds\Bigg\} = 0, \end{aligned} \tag{9}$$

which, since $\tilde{p} \in S^1_{ad} \times S^2_{ad}$, becomes:

$$\begin{aligned} a(\tilde{p},\tilde{p}) = \mathrm{Re}\Bigg\{ &\sum_{E=1,2} -\frac{i}{\rho_0\omega}\int_{\Omega_E}(\nabla\tilde{p}_E\cdot\overline{\nabla\tilde{p}_E} - k^2\tilde{p}_E\overline{\tilde{p}_E})\,d\Omega \\ &- \sum_{E=1,2}\frac{1}{2}\int_{\partial_Z\Omega_E}\left(Z_EL_v[\tilde{p}_E]\overline{L_v[\tilde{p}_E]} + \frac{1}{Z_E}\tilde{p_E}\overline{\tilde{p}_E}\right)ds\Bigg\} = 0. \end{aligned} \tag{10}$$

Therefore, the real part of (10) yields:

$$-\sum_{E=1,2}\int_{\partial_Z\Omega_E}\left(Z_E L_v[\tilde{p}_E]\overline{L_v[\tilde{p}_E]}+\frac{1}{Z_E}\tilde{p_E}\overline{\tilde{p}_E}\right)ds=0. \tag{11}$$

The last equation shows that $\tilde{p}_E=0$ and $\mathbf{n}_E^T\cdot\nabla\tilde{p}_E=0$ throughout $\partial_Z\Omega_E$. Reintroducing that result into (7), one gets:

$$\mathrm{Re}\left\{\sum_{E=1,2}\int_{\partial_p\Omega_E}(\tilde{p}_E)\cdot\overline{L_v[\delta p_E]}ds+\sum_{E=1,2}\int_{\partial_v\Omega_E}\overline{L_v[\tilde{p}_E]}\delta p_E ds\right.$$
$$\left.+\frac{1}{2}\int_\Gamma((\tilde{p}_1-\tilde{p}_2)\cdot\overline{L_v[\delta p_1-\delta p_2]}+\overline{L_v[\tilde{p}_1+\tilde{p}_2]}\cdot(\delta p_1+\delta p_2))\,ds\right\}=0. \tag{12}$$

Since $\delta p_E$ and its normal gradient are arbitrary, this leads to $\tilde{p}_E=0$ over $\partial_P\Omega_E$, to $L_v[\tilde{p}_E]=0$ over $\partial_v\Omega_E$ and to the transmission continuity (4) for $\tilde{p}_E$. Therefore, $\tilde{p}_E$ verifies the initial Helmholtz reference problem with homogeneous conditions, i.e. $\tilde{p}_E$ is equal to zero, which proves the uniqueness of the solution of (6) and, consequently, the equivalence of (6) with (2), (3), (4).

Since the reverse of that implication is obvious, the equivalence between the reference problem (2), (3), (4) and the variational problem (6) is proven.

This result is similar to that given in Ref. 27 except that in the case of structures the uniqueness of the solution results from the hysteretic damping introduced into the constitutive law (which means that the structure dissipates energy). In acoustics, damping is localized primarily at the boundaries and taken into account by the Robin equation (3). This is clearly the case in buildings, where absorption takes place in insulation materials. Therefore, the normal impedance, especially its real part $\mathrm{Re}(Z_E)$, is essential because it is what ensures the uniqueness of the solution. Of course, any type of damping can be taken into account in the reference problem. In that case, the wave number $k$ has a complex part, which leads to a new term associated with inner dissipation within the cavity, as in Ref. 27. The conclusion of the proof, however, remains the same.

The bilinear form $a(p,\delta p)$ can be decomposed into a Hermitian part $a_H(p,\delta p)$ and an anti-Hermitian part $a_A(p,\delta p)$. One can easily prove that the Hermitian part takes the form $a_H(p,\delta p)=W_Z^{(1)}(p_1)+W_Z^{(2)}(p_2)$ with $W_{Z(p_E)}^{(E)}=\mathrm{Re}\{-\int_{\partial_Z\Omega_E}p_E.\overline{\mathbf{v_E}}.\mathbf{n_E}ds\}$ (see Ref. 35). Therefore, (6) becomes:

$$\begin{aligned}&\text{Find } p\in S_{ad}^1\times S_{ad}^2 \text{ such that}\\ &\delta(W_Z^{(1)}(p_1)+W_Z^{(2)}(p_2))+\langle p,\delta p\rangle=(l_d,\delta p),\quad \forall\,\delta p\in S_{ad}^1\times S_{ad}^2,\end{aligned} \tag{13}$$

where $(l_d,\cdot)$ is the linear form associated with the acoustic boundarys conditions, $\langle\cdot,\cdot\rangle$ is the anti-Hermitian part of $a(p,\delta p)$, and $\delta(\square)$ is a small variation of the quantity $\square$. One can see that the Hermitian part of the formulation is associated directly with the damping introduced in $\partial_Z\Omega_E$. Consequently, this quantity must be calculated with care because it is what ensures the uniqueness of the solution.

### 2.3. *The discretized problem*

In order to solve (6), one must use approximations $p_E^a$ for each subcavity $\Omega_E$. These approximations must be chosen in $S_{ad}^{a,E} \subset S_{ad}^E$. Therefore, the discretized version of (6) is:

$$\begin{aligned} &\text{Find } p^a = (p_1^a, p_2^a) \in S_{ad}^{a,1} \times S_{ad}^{a,2} \text{ such that} \\ &\delta(W_Z^{(1)}(p_1^a) + W_Z^{(2)}(p_2^a)) + \langle p^a, \delta p^a \rangle = (l_d, \delta p^a), \quad \forall\, \delta p^a \in S_{ad}^{a,1} \times S_{ad}^{a,2}. \end{aligned} \tag{14}$$

In the VTCR, the approximations $p^a$ are sought in the space of the propagative waves: $p_E^a(\mathbf{x}) = \int_{C_E} A_E^a(\mathbf{k_E}) \cdot e^{i\mathbf{k_E}\cdot\mathbf{x}} dC_E$, where $A_E^a$ denotes the amplitude of a wave, $\mathbf{k_E}$ is the wave vector in $\Omega_E$ and $C_E$ is the circle which corresponds to all the possible wave propagation directions in the 2D cavity. One can see that in the VTCR the solution is considered to be a superposition of propagative waves. If necessary, other types of waves can be introduced (for example, see Ref. 31). Furthermore, the presence of the superscript $a$ in $A_E^a$ alone shows that the VTCR approximates (and, therefore, discretizes) only the amplitudes of the waves, but not their spatial shapes. Therefore, the VTCR belongs to the multiscale category of numerical approaches in which only the slowly oscillating quantities are discretized. Finally, one can observe that all the propagative waves are taken into account thanks to the integral distribution of their directions over the whole domain. This is important because the wave propagation directions are not known *a priori*.

$A_E^a(\mathbf{k_E})$ represents the discretized amplitudes of the propagative waves over the circle $C_E$. This discretization can take many forms: $A_E^a(\mathbf{k_E})$ can be sought as a piecewise constant function

$$p_E^a(\mathbf{x}) = \int_{C_E} A_E^a(\mathbf{k_E}) e^{i\mathbf{k_E}\cdot\mathbf{x}} dC_E = \sum_{l=1}^{L_E} a_E^l \int_{C_E^l} e^{i\mathbf{k_E}\cdot\mathbf{x}} dC_E \tag{15}$$

or a piecewise Dirac function

$$p_E^a(\mathbf{x}) = \int_{C_E} A_E^a(\mathbf{k_E}) e^{i\mathbf{k_E}\cdot\mathbf{x}} dC_E = \sum_{l=1}^{L_E} a_E^l e^{i\mathbf{k_E^l}\cdot\mathbf{x}}. \tag{16}$$

Therefore, the approximate solution is sought as $p_E^a(\mathbf{x}) = \mathbf{a}_E^T.\varphi_E(\mathbf{x})$, where $\varphi_E = [\varphi_{E,1}\varphi_{E,2}\cdots\varphi_{E,L_E}]^T$ is the vector of the shape functions and $\mathbf{a_E}$ the vector of the associated amplitudes. In the case of Approximation (15) $\varphi_{E,l}(\mathbf{x}) = \int_{\theta_{l-\frac{1}{2}}}^{\theta_{l+\frac{1}{2}}} e^{i\mathbf{k}_E(\theta)\cdot\mathbf{x}} d\theta$, and in the case of Approximation (16) $\varphi_{E,l}(\mathbf{x}) = e^{i\mathbf{k}_E(\theta_l)\cdot\mathbf{x}}$. In both cases, $S_{ad}^{a,E} = \text{Vect}\{\varphi_{E,l}(\mathbf{x})\}_{l\in\{1,\ldots,L_E\}}$.

Introducing (15) or (16) into (14), one gets a set of $L_1 + L_2$ algebraic equations whose solution is the vector of generalized amplitudes $\mathbf{a} = \begin{bmatrix}\mathbf{a}_1 \\ \mathbf{a}_2\end{bmatrix}$, of size $L_1 + L_2$, which verifies:

$$\begin{bmatrix} \underline{\mathbf{K}}_{11} & \underline{\mathbf{K}}_{12} \\ \underline{\mathbf{K}}_{21} & \underline{\mathbf{K}}_{22} \end{bmatrix} \cdot \begin{bmatrix} \mathbf{a}_1 \\ \mathbf{a}_2 \end{bmatrix} = \begin{bmatrix} \mathbf{b}_1 \\ \mathbf{b}_2 \end{bmatrix}, \tag{17}$$

where $\underline{\mathbf{K}}$ and $\mathbf{b}$ denote respectively the matrix of the bilinear forms and the vector of the linear form of variational formulation (6).

The resolution of (17) followed by the back-substitution of the result into function $p_E^a(\mathbf{x})$ leads to the numerical solution of the acoustic problem.

Several remarks can be made:

- Since the variational formulation is not symmetrical, the VTCR is not a discontinuous Galerkin method.
- Since the complex rays $\{\varphi_{E,l}(\mathbf{x})\}_{l\in\{1,\ldots,L_E\}}$ are defined over the entire acoustic subcavity $\Omega_E$, the matrices of the model are fully populated. However, in the case of more than two cavities, the off-diagonal submatrix $[\underline{\mathbf{K}}]_{ij}$ is zero if Cavity $i$ is not connected to Cavity $j$.
- Since the complex rays depend implicitly on the frequency, so do the matrices of the model. Therefore, they cannot be partitioned into frequency-independent submatrices. However, strategies have been developed in order to calculate the solution over a range of frequencies without calculating the response at each frequency (see Ref. 32).
- The use of piecewise constant functions in the VTCR to approximate the amplitudes of the waves is more involved numerically than the use of piecewise Dirac functions. In the latter case, many integrations can be carried out analytically. However, in the case of wavebands, semi-analytical strategies can be used, as in Ref. 27. These strategies are based on the approximation of variable angular functions as piecewise angular functions which can be integrated analytically.
- As mentioned previously, no Lagrange multiplier is required in order to ensure the continuity of the solution. This is taken into account automatically in the variational formulation (6).
- Two different approaches can be used and will be illustrated in the following examples: the $h$-approach (which consists in keeping the number of waves constant and decreasing the size of the subcavities $\Omega_E$, hence the denomination $h$ in reference to the FE technique in which the mesh is refined), and the $p$-approach (which consists in keeping the number of subcavities $\Omega_E$ constant and increasing the number of waves $L_E$ in each subcavity, hence the denomination $p$ in reference to the FE technique in which the polynomial degree of the shape functions is increased). With each approaches, the shape functions are $\int_{C_E^l} e^{i\mathbf{k_E}\cdot\mathbf{x}} dC_E$ (see 15) or $e^{i\mathbf{k_E^l}\cdot\mathbf{x}}$ (see 16).

### 2.4. *Example of convergence*

There are many examples in the literature showing the convergence of the VTCR (see, e.g. Refs. 27–34). Here we present another example of the convergence of the method which takes into account the impedance $Z$ along boundary $\partial_Z\Omega$. This example will be used in the following sections.

The domain $\Omega$ is a square acoustic cavity of width $L$ ($\rho_0 = 1,3\,\mathrm{kg}\cdot\mathrm{m}^{-3}$ and $c_0 = 330\,\mathrm{m}\cdot\mathrm{s}^{-1}$) subjected along all four sides to a Robin condition with $Z = \rho_0 c_0$ and a prescribed excitation $h_d$ such that the exact solution $p_{\mathrm{ex}}(\mathbf{x}) = e^{-i\mathbf{k}_e\cdot\mathbf{x}}$ (with $\mathbf{k}_e = k[\cos\theta_{\mathrm{ex}}, \sin\theta_{\mathrm{ex}}]^T$) corresponds to the propagative wave in direction $\theta_{\mathrm{ex}} = 12°$. Two circular frequencies were considered for the excitation so that $kL = 80$ (which corresponds to

about 13 wavelengths in the cavity) and $kL = 160$ (which corresponds to about 25 wavelengths in the cavity), respectively. The approximations were based on piecewise constant functions. In applying the VTCR, as mentioned in the last remark of Sec. 2.3, two different approaches were used: the $h$-approach and the $p$-approach. For the VTCR $h$-approach, the geometry (here a simple square) was divided into squares of width $h$ such that $L/h = n$, $n$ being a positive integer. For the VTCR $p$-approach, the cavity was either considered as a whole or divided into two rectangular subcavities of equal size.

Once the exact solution is known, it is possible to calculate the actual error $\|p - p_{\text{ex}}\|_{L^2(\Omega)}$. Figures 2 and 3 show the convergence curves of the actual relative error $\|p - p_{\text{ex}}\|_{L^2(\Omega)}/\|p_{\text{ex}}\|_{L^2(\Omega)}$ for the FEM, the VTCR $h$-approach and the VTCR $p$-approach as a function of the number of DOFs. Several remarks can be made about these figures:

- The resolution of an acoustic problem with a Robin condition using the VTCR presents no difficulty. The approximate solution converges towards the exact solution.
- The VTCR $p$-approach produces more accurate results with fewer DOFs. This is even more the case when the frequency increases.
- The FEM requires a huge number of DOFs in order to alleviate the pollution effect. For example, for $kl = 160$, keeping $kL.(kh)^2$ below 1 requires 1000 elements along each edge (see Ref. 3). The VTCR $h$-approach suffers less from the pollution effect because it uses oscillating wave functions. The comparison between the VTCR solution with 32 wavebands and the VTCR solution with 52 wavebands shows that the pollution decreases when the number of waves increases.

This simple numerical test agrees with the results already presented in Ref. 36: The convergence of the $p$-approach is exponential, whereas the convergence of the $h$-approach is slower. This is the reason why the VTCR leads to good results with only a few DOFs.

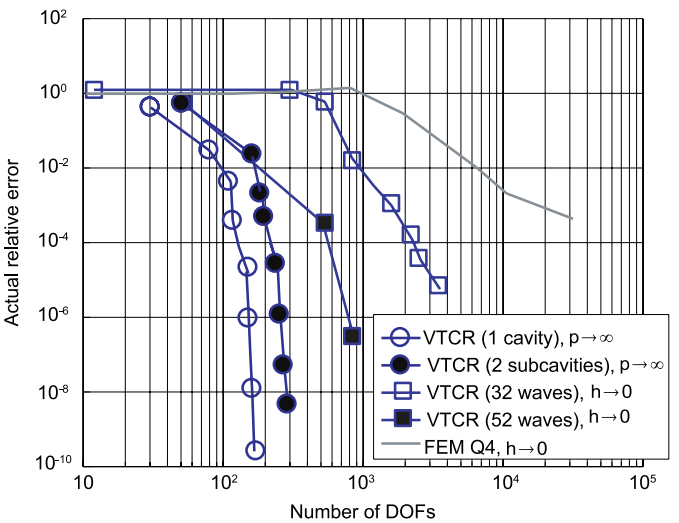


Fig. 2. Example of a square (see Sec. 2.4). Comparison between the VTCR and the FEM. $kL = 80$.

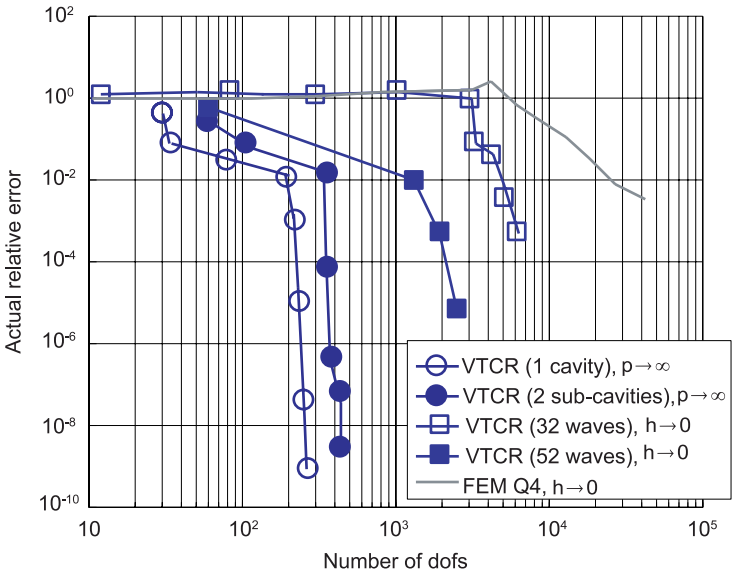


Fig. 3. Example of a square (see Sec. 2.4). Comparison between the VTCR and the FEM. $kL = 160$.

## 3. The Error Indicator

### 3.1. *Construction of an error indicator for the VTCR*

As mentioned in Sec. 2, it is very important to quantify the accuracy of the approximate solution. Using the actual error would be an interesting way to do that, but it is impracticable because the problem (2), (3), (4) usually has no analytical solution. Furthermore, the definition of an error indicator for each subcavity $\Omega_E$ is a difficult task because some subcavities $\Omega_E$ may not be connected to the boundary $\partial\Omega$ at all and, therefore, it is impossible to verify in these subcavities an equation such as (3), which is attached only to the boundaries and is the only reliable equation. The only way to assess the accuracy of the approximate solution in a subcavity $\Omega_E$ is to verify the transmission condition (4) with all the other subcavities in its vicinity. However, the verification of such an equation is hampered by the fact that the solutions in these neighboring subcavities are not exact solutions.

The error indicator we propose in this paper is based on the total energy of each $\Omega_E$, denoted $E_{T,\Omega_E}$, i.e. the sum of the time averages of the kinematic and potential energies, and is equal to the dimensionless quantity:

$$I_\Omega = \max_E I_{\Omega_E} = \max_E \frac{E_{T,\Omega_E}(p_E^a - p_E^{pv})/\mathrm{mes}(\Omega_E)}{\sum_E E_{T,\Omega_E}(p_E^a)/\mathrm{mes}(\Omega)}, \tag{18}$$

where $\mathrm{mes}(\Omega)$ and $\mathrm{mes}(\Omega_E)$ designate the measures of $\Omega$ and $\Omega_E$, respectively, and $p_E^{pv}$ refers to the solution of the problem in $\Omega_E$ under prescribed pressure and velocity along the boundaries of $\Omega_E$ which correspond to the pressure and the velocity in all the $\Omega_{E'}$ adjacent to $\Omega_E$. This is achieved by applying the variational formulation (6) to $\Omega_E$, with both the

pressure and the velocity prescribed along the same boundary thanks to the additional term

$$\mathrm{Re}\left\{\frac{1}{2}\int_{\partial_{pv}\Omega_E}((p_E - p_{dE})\cdot\overline{L_v[\delta p_E]} + \overline{L_v[p_E] - v_{dE}}\cdot\delta p_E)\,ds\right\}.$$

One can see that $I_\Omega$ measures the total energy of the relative difference between the approximate solution and the exact solution of the problem with prescribed pressure and velocity, and quantifies the maximum global error in energy per subcavity. Therefore, it quantifies the consistency of the calculated solution in $\Omega_E$ and, thus, in $\Omega$. Indeed, a too large $I_{\Omega_E}$ indicates that the data at the boundaries of $\Omega_E$ are incompatible and, therefore, were poorly calculated.

Furthermore, since $I_{\Omega_E}$ is defined in each subcavity $\Omega_E$, it can be used to determine the locations in which the discretization must be refined, leading to an adaptive version of the VTCR which will be presented in the next section.

### 3.2. *Assessment of the VTCR error indicator for a highly directional example*

First, let us go back to the previous numerical example (see Sec. 2.4): A square acoustic cavity of width $L(\rho_0 = 1,3\,\mathrm{kg}\cdot\mathrm{m}^{-3}$ and $c_0 = 330\,\mathrm{m}\cdot\mathrm{s}^{-1})$ subjected along all four sides to a Robin condition with $Z = \rho_0 c_0$ and a prescribed excitation $h_d$ such that the exact solution $p_{\mathrm{ex}}(\mathbf{x}) = e^{-i\mathbf{k}_e\cdot\mathbf{x}}$ (with $\mathbf{k}_e = k[\cos\theta_{\mathrm{ex}}, \sin\theta_{\mathrm{ex}}]^T$) corresponds to the propagative wave in direction $\theta_{\mathrm{ex}} = 12°$ at two circular frequencies determined by $kL = 80$ and $kL = 160$, respectively. Therefore, the exact wave amplitude is $A_{\mathrm{ex}}(\theta) = \delta(\theta - \theta_{\mathrm{ex}})$. Figure 4 shows the exact solution of this first numerical example. This example is interesting because the problem is highly directional with respect to the directions of propagation of the waves.

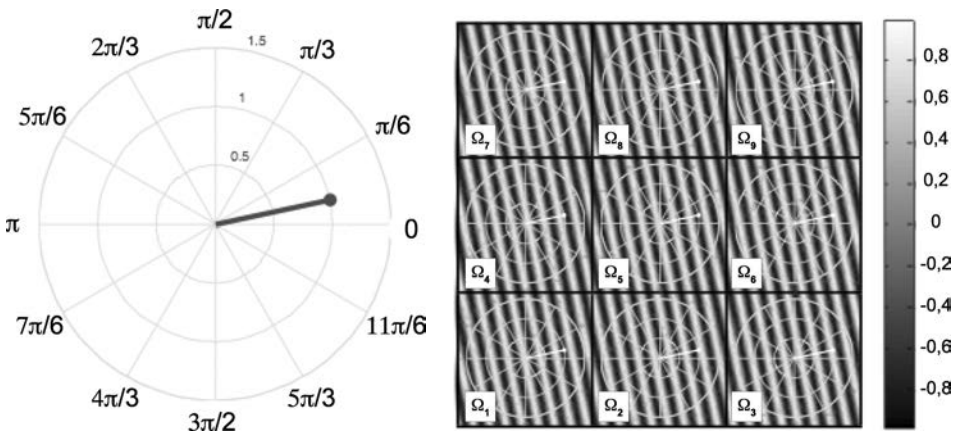


(a) (b)

Fig. 4. The exact solution of the first example (see Sec. 3.2). (a) The wave amplitude $A_{\mathrm{ex}}(\theta)$ and (b) the real part of the pressure.

The problem was solved with the VTCR using a uniform decomposition of $\Omega$ into $9 = 3 \times 3$ square subcavities (see Fig. 4). The solution was obtained by extending (6) to the 9 subcavities.

In order to illustrate the effectiveness of error indicator $I_\Omega = \max_E I_{\Omega_E}$, Fig. 5 shows how it compares with the actual relative errors in energy defined in each $\Omega_E$ (obtained by substituting $p_{\text{ex}}$ for $p_E^{pv}$ in (18)).

One can see that error indicator $I_\Omega = \max\limits_E I_{\Omega_E}$ (18) is a valid measure of the quality of the calculated solution. Indeed, $I_{\Omega_E}$ is very close to the actual relative error in energy for each subcavity and at each frequency considered. This numerical test shows that $I_\Omega$ (18) can provide an indication of the accuracy of the solution in an example whose solution is highly directional.

On these curves, one can see that sometimes the errors stop decreasing beyond a certain large number of DOFs. This is a known behavior which is present in many strategies using oscillating functions as the approximate fields (see Refs. 20, 23, 26 and 34). The problem occurs when the number of waves being used becomes too large: The waves are so close to one another that the computer, even using double-precision arithmetics, cannot tell the difference numerically. Then, the conditioning number reaches the limit of the machine capacity and the process ceases to converge.

### 3.3. *Assessment of the VTCR error indicator for an example with a continuous wave distribution*

Now let us consider the numerical example of a square acoustic cavity of width $L$ ($\rho_0 = 1,3\,\text{kg}\cdot\text{m}^{-3}$ and $c_0 = 330\,\text{m}\cdot\text{s}^{-1}$) subjected along all four sides to a Robin condition with $Z = \rho_0 c_0$ and a prescribed excitation $h_d$ such that exact wave amplitude at the two circular frequencies determined by $kL = 80$ and $kL = 160$ is

$$A_{\text{ex}}(\theta) = \begin{cases} (1+i)\sin(4\theta) & \text{for } \theta \in \left]-\dfrac{\pi}{4};\dfrac{\pi}{2}\right[ \\ 0 & \text{else} \end{cases}. \tag{19}$$

Figure 6 shows the exact solution of this second numerical example for $kL = 80$. This example is interesting because it involves a continuous distribution of waves rather than some discrete directions of propagation. Again, in order to solve the problem using the VTCR, we used a uniform distribution and divided $\Omega$ into $9 = 3 \times 3$ square subcavities. Figure 7 shows the error indicator (18) in each subcavity $\Omega_E$ compared with the actual relative error in energy. One can see again that error indicator $I_\Omega = \max\limits_E I_{\Omega_E}$ (18) is a valid measure of the quality of the calculated solution. This numerical test shows that $I_\Omega$ (18) can provide an indication of the accuracy of the solution in an example whose solution presents a continuous angular wave distribution.

In this example, one can observe that the error is distributed relatively evenly among the subcavities. This is a consequence of the VTCR discretization, which is the same in all the $\Omega_E$. If one wants to use a coarser discretization in one of the $\Omega_E$ (which the VTCR

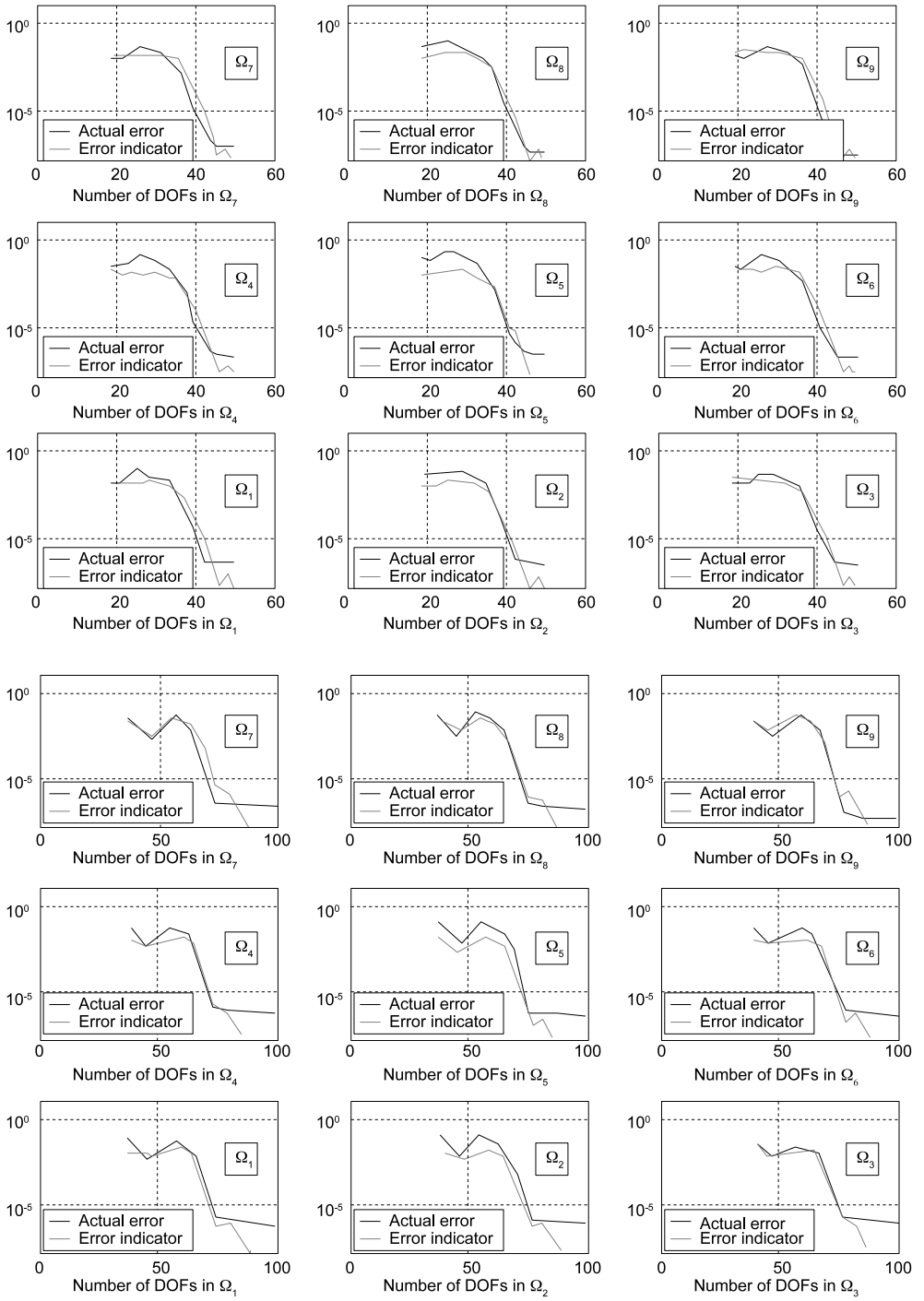


Fig. 5. Comparison between error indicator (18) and the actual relative error in energy for the first example with $A_{\mathrm{ex}}(\theta) = \delta(\theta - \theta_{\mathrm{ex}})$ (see Sec. 3.2 and the solution and the discretization of Fig. 4). Two circular frequencies such that $kL = 80$ (nine top curves) and $kL = 160$ (nine lower curves) are considered.

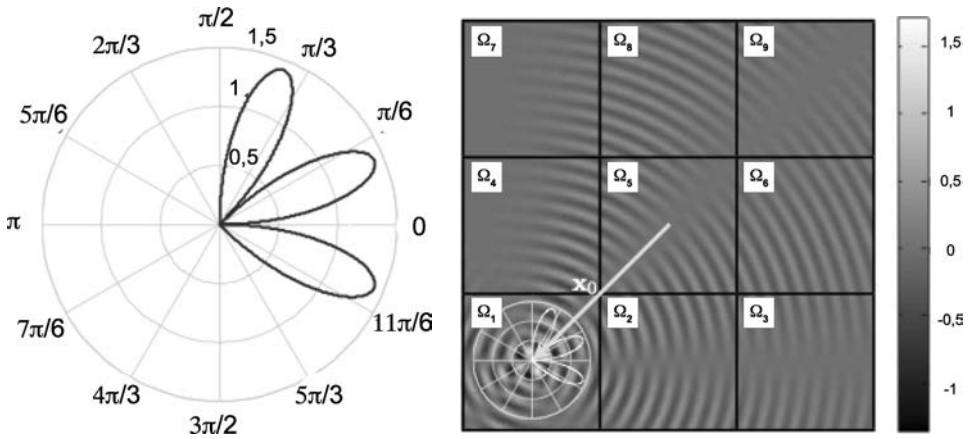


(a) (b)

Fig. 6. The exact solution of the second example (see Sec. 3.3). (a) The wave amplitude $|A_{\text{ex}}(0)|$ and (b) the real part of the pressure.

allows, see Ref. 34), the error would be localized in that subcavity. Of course, the error indicator $I_{\Omega_E}$ would reflect that situation.

## 4. An Adaptive Version of the VTCR

### 4.1. *Presentation of the method*

It is clear from Sec. 2 that the unknowns of the VTCR are the amplitudes $A_E^q(\theta)$ of the waves traveling in all directions $\theta \in [0; 2\pi[$ of the 2D acoustic cavity. Of course, these amplitudes are not necessarily uniformly distributed: For specific internal cavity shapes whose boundaries guide the waves, the amplitudes can be sparsely distributed in some angular directions and densely distributed in others. Therefore, in the case of a piecewise constant angular approximation for the amplitudes (15), it would surely be advantageous to use different discretizations depending on the propagation direction.

The idea of the adaptive version of the VTCR stemmed from that remark. The objective is to enable one to calculate the VTCR using different angular discretizations: A refined angular discretization when the wave amplitudes are densely distributed and a coarse angular discretization when the amplitudes are sparsely distributed. Therefore, the process is completely analogous to that used in the adaptive FEM[37] and consists of three steps (see Fig. 8):

(1) In the first step, a global analysis of the problem is carried out using a uniform, low-density angular wave distribution based on a coarse angular grid $\tau^M$ (see Fig. 8(a)).
(2) The objective of the second step is to calculate the proper angular discretization. The quality of the approximation of the first step is quantified using error indicator $I_\Omega$ (18), which indicates whether a new angular mesh is necessary. If that is the case, a local analysis is performed in subcavity $\Omega_E$ using a refined angular grid $\tau^m$ and applying the

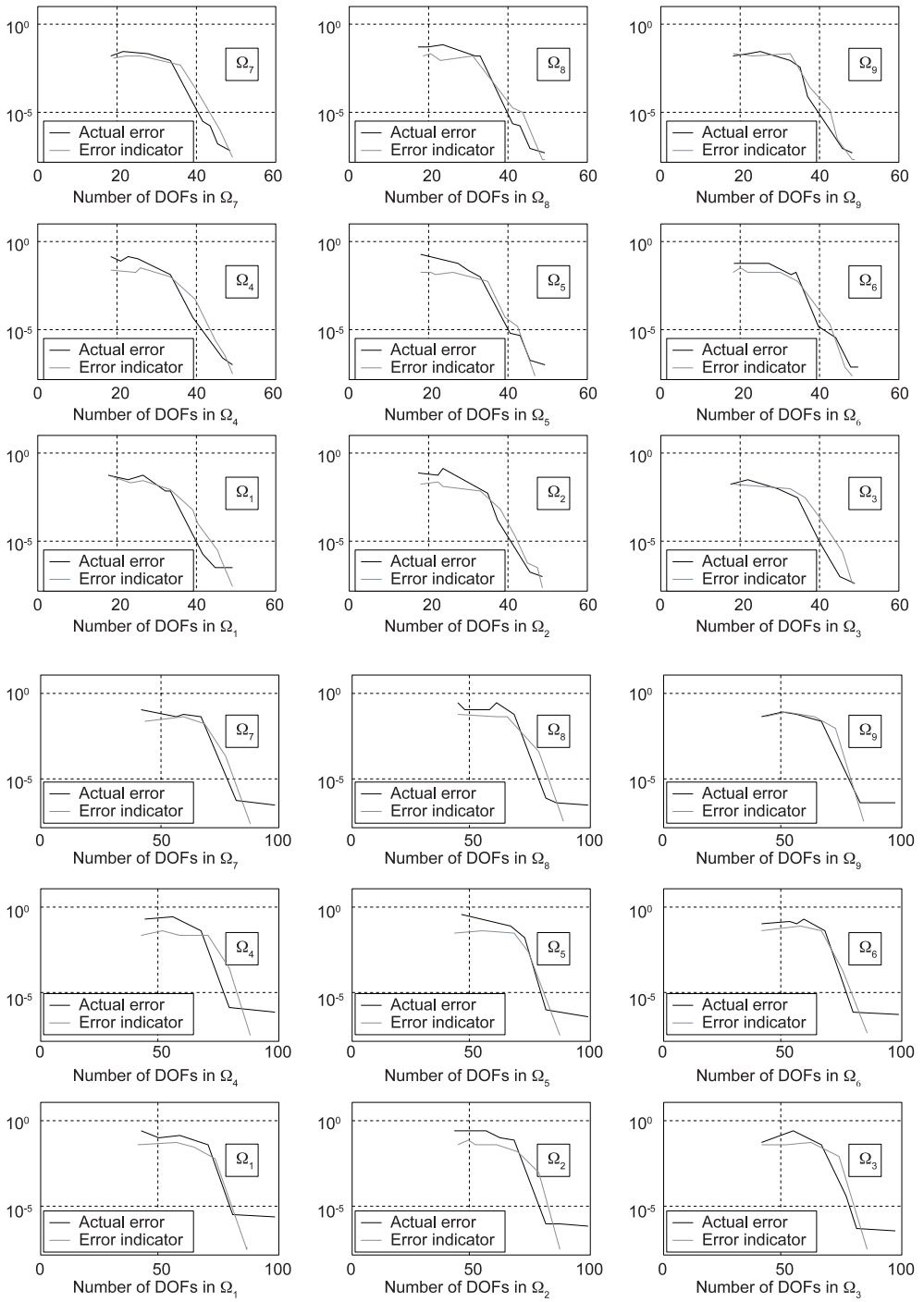


Fig. 7. Comparison between error indicator (18) and the actual relative error for the second example with $A_{\text{ex}}(\theta) = (1+i)\sin(4\theta)$ if $\theta \in ]-\pi/4;\pi/2[$ and $A_{\text{ex}}(\theta) = 0$ otherwise (see Sec. 3.3 and the solution and the discretization of Fig. 6). Two circular frequencies such that $kL = 80$ (nine top curves) and $kL = 160$ (nine lower curves) are considered.

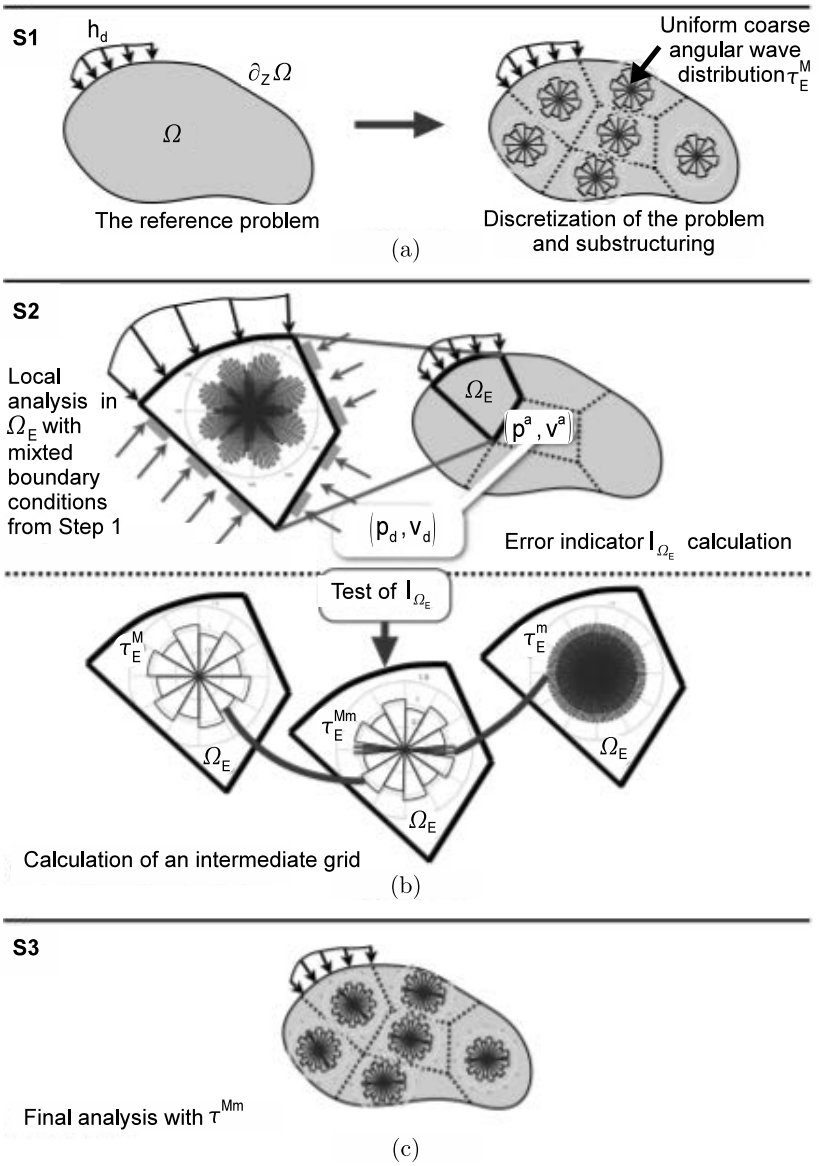


Fig. 8. The three steps of the adaptive VTCR strategy. (a) Step 1, (b) Step 2 and (c) Step 3.

boundary conditions obtained from Step 1 along the edges. This leads to a new angular grid $\tau^{Mm}$ which is intermediate between the coarse angular grid $\tau^M$ and the refined angular grid $\tau^m$ (see Fig. 8(b)).

(3) The third step is a new complete calculation using angular grid $\tau^{Mm}$ (see Fig. 8(c)).

If the accuracy of the last calculation is insufficient, the procedure can be repeated until the desired accuracy is reached.

For the second step, it can be useful to set two limit levels $m_0$ and $m_1$: if $I_{\Omega_E} < m_0$, the quality of the solution is considered to be good and no rediscretization of subcavity $\Omega_E$ is necessary. If $m_0 < I_{\Omega_E} \leq m_1$, the error is moderate, but still too high and a new refined angular discretization is necessary. If $m_1 < I_{\Omega_E}$, the solution is seriously inaccurate and the boundary conditions of $\Omega_E$ must be recalculated more precisely, which requires a new first step (see Fig. 8(a)). In practice, one often chooses $m_0 = 10\%$ and $m_1 = 40\%$.

### 4.2. *Calculation of the adapted angular discretization*

As explained before, a large $I_{\Omega_E}$ indicates a poor solution in $\Omega_E$ due to too coarse an angular discretization of the wave amplitudes. A new adapted angular discretization is required. In order to obtain that, one uses a refined angular grid $\tau^m$ in $\Omega_E$. The pressures and velocities calculated in Step 1 are prescribed along the boundaries (except if an edge of $\Omega_E$ corresponds to the boundary of $\Omega$, in which case the boundary conditions of the initial problem are used). Then, an energy criterion based on the amplitudes of the waves is used to determine which angular wave directions in $\Omega_E$ are important and require the refined discretization. If the propagation interval $[0; 2\pi[$ is discretized into $L_E$ angular sectors, the criterion is defined with a parameter $\eta$ as follows:

- If the amplitude of the wave verifies $|a_E^l|^2 < \eta a_{\max}^2$, then the angular interval $[\theta_{l-\frac{1}{2}}; \theta_{l+\frac{1}{2}}[$ can be discretized using the coarse angular grid $\tau^M$.
- If the amplitude of the wave verifies $|a_E^l|^2 > \eta a_{\max}^2$, then the angular interval $[\theta_{l-\frac{1}{2}}; \theta_{l+\frac{1}{2}}[$ can be discretized using the refined angular grid $\tau^m$.

The final angular discretization is defined using the appropriate grid ($\tau^M$ or $\tau^m$), denoted $\tau^{Mm}$, for each angular sector of $\Omega_E$ in $[0; 2\pi[$. In practice, one often chooses $\eta = 0.1$.

### 4.3. *Selection of the coarse and refined angular discretizations*

A key point of the adaptive version of the VTCR is the choice of the coarse and refined angular discretizations, i.e. the number of waves to be used in directions where the evolution is smooth or irregular, respectively. An important point which must be understood is that it is not necessary to use the same number of DOFs in acoustic cavities of different sizes. Indeed, more waves are required in large cavities than in small cavities for similar accuracy results. Thus, an interesting heuristic criterion to define the number of waves to be used in $\Omega_E$ is

$$L_E = [T \cdot k \cdot \mathrm{diam}\,(\Omega_E)], \tag{20}$$

where $T$ is a positive real number, $\mathrm{diam}(\Omega_E)$ the diameter of $\Omega_E$, and $[\square]$ the integer part of $\square$. All the examples presented in Refs. 28–34 show that such a criterion guarantees similar accuracy with the VTCR in all the $\Omega_E$ for a large range of frequencies.

Therefore, for the coarse and refined discretizations, the angular size of the grids is defined as

$$\begin{aligned} \tau_E^M : \Delta\theta_E^M &= 2\pi/[T^M \cdot k \cdot \mathrm{diam}(\Omega_E)] \\ \tau_E^m : \Delta\theta_E^m &= 2\pi/[T^m \cdot k \cdot \mathrm{diam}(\Omega_E)]. \end{aligned} \tag{21}$$

Having considered numerous examples, the authors feel that $T^M \in [0; 0.8]$ and $T^m \in [1; 2]$ are good choices. The small $T^M$ used in the coarse angular discretization enables one to use only a few waves in directions which are not significant in terms of energy while the large $T^m$ used in the refined angular discretization enables the use of many waves in directions which are significant in terms of energy for the solution.

An important consideration is the need for very stable coefficients $a_E^l$. Indeed, problems can occur when the number of waves is too large, leading to ill-conditioning of the matrices and an unstable solution $a_E^l$ even though solution $p_E$ is good. In order to improve robustness, one must use a regularization technique (see Ref. 35). The purpose of such a technique is to find a regularized solution of problem (17):

$$\begin{bmatrix} \underline{\mathbf{K}}_{11} + \lambda_p \underline{\mathbf{H}}_1 & \underline{\mathbf{K}}_{12} \\ \underline{\mathbf{K}}_{21} & \underline{\mathbf{K}}_{22} + \lambda_p \underline{\mathbf{H}}_2 \end{bmatrix} \cdot \begin{bmatrix} \mathbf{a}_{1,\lambda_p} \\ \mathbf{a}_{2,\lambda_p} \end{bmatrix} = \begin{bmatrix} \mathbf{b}_1 \\ \mathbf{b}_2 \end{bmatrix}, \tag{22}$$

where $\underline{\mathbf{H}}_E$ is a regularization operator which represents the norm of the second $\theta$-derivative of the amplitudes $a_E(\theta)$, and $\lambda_p$ a weighting coefficient. This technique will be developed in a forthcoming paper.

## 5. Assessment of the Performance of the Adaptive Version of the VTCR

In this section, the performance of the adaptive VTCR is evaluated based on two benchmark acoustic problems considered at two different frequencies each. These problems are formulated in such a way that the exact solutions are known, which enables one to calculate the exact convergence curves.

### 5.1. *Numerical results of an example based on a propagative wave*

Let us go back to the first numerical example of Sec. 3.2: A square acoustic cavity of width $L$ ($\rho_0 = 1,3\,\mathrm{kg\cdot m^{-3}}$ and $c_0 = 330\,\mathrm{m\cdot s^{-1}}$) subjected along all four sides to a Robin condition with $Z = \rho_0 c_0$ and a prescribed excitation $h_d$ such that the exact solution $p_{\mathrm{ex}}(\mathbf{x}) = e^{-i\mathbf{k}_e\cdot\mathbf{x}}$ (with $\mathbf{k}_e = k[\cos\theta_{\mathrm{ex}}, \sin\theta_{\mathrm{ex}}]^T$) corresponds to the propagative wave in direction $\theta_{\mathrm{ex}} = 12^\circ$ at two circular frequencies such that $kL = 80$ and $kL = 160$, respectively. The problem was solved using a $3 \times 3$ spatial discretization of $\Omega$. The exact solution is shown in Fig. 4. Again, this example is interesting because it shows the behavior of the adaptive version of the VTCR for an example in which the solution being sought is highly directional in terms of the wave propagation.

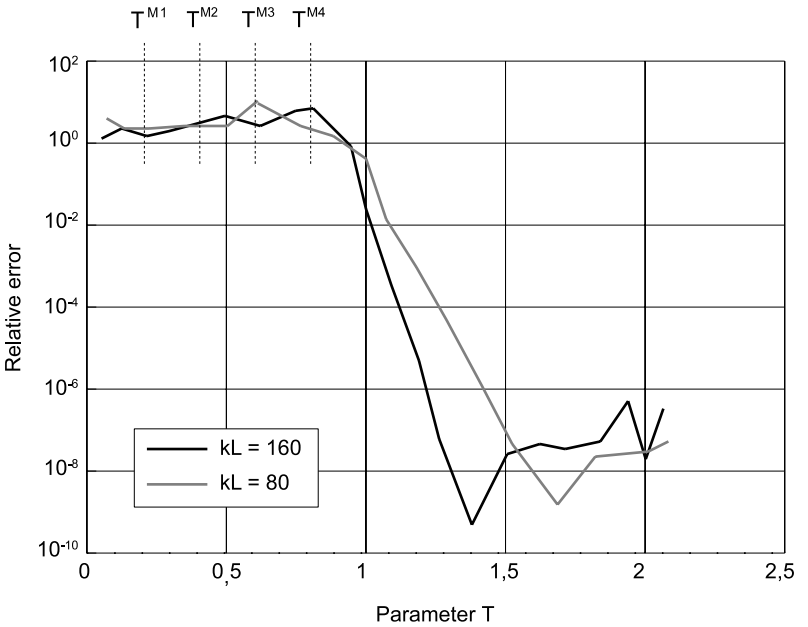


Fig. 9. The relative error in $L^2$ norm as a function of parameter $T$ (20) in subcavity $\Omega_5$ (see Fig. 4) for the first adaptive example (see Sec. 5.1).

Formulae (21) determine the number of waves to be used in the coarse and refined angular discretizations based on the definitions of $\tau_E^m$ and $\tau_E^M$. Figure 9 shows the convergence curves as functions of parameter $T$ (see (20)) for subcavity $\Omega_5$ (see Fig. 4), which is the most critical subcavity because it is attached to no reliable boundary condition. This curve shows that the heuristic law (20) works because the number of waves to be used is independent of the frequency being considered. Indeed, the parameter $T$ to be used to achieve a given error level is almost the same. The behavior of the curves corresponding to the other subcavities $\Omega_E$ is similar.

In order to evaluate the convergence of the strategy, we tested four values of parameter $T^M$: $T^{M1} = 0.2$, $T^{M2} = 0.4$, $T^{M3} = 0.6$ and $T^{M4} = 0.8$ (see Fig. 9). The convergence of the VTCR was tested by making $T^m \to \infty$. The energy criterion was used as explained in Sec. 4.2 to determine the dominant propagation directions in terms of energy for the solution. The results are compared to the nonadaptive VTCR with a uniform angular wave discretization in Fig. 10.

These curves show that the convergence rate of the adaptive VTCR is much better. For this example in which the solution is highly directional, this technique is very efficient. Furthermore, one can see that the efficiency was highest with the coarsest angular discretization. This is due to the shape of the exact solution being sought. Indeed, the wave propagating in direction $\theta_{\text{ex}} = 12^\circ$ is the only wave needed. The adaptive procedure detects that specificity and focuses the refined angular discretization on that angle. The coarse discretization concerns all the other directions, which are not needed. Therefore, this coarse discretization should be as coarse as possible, or even eliminated.

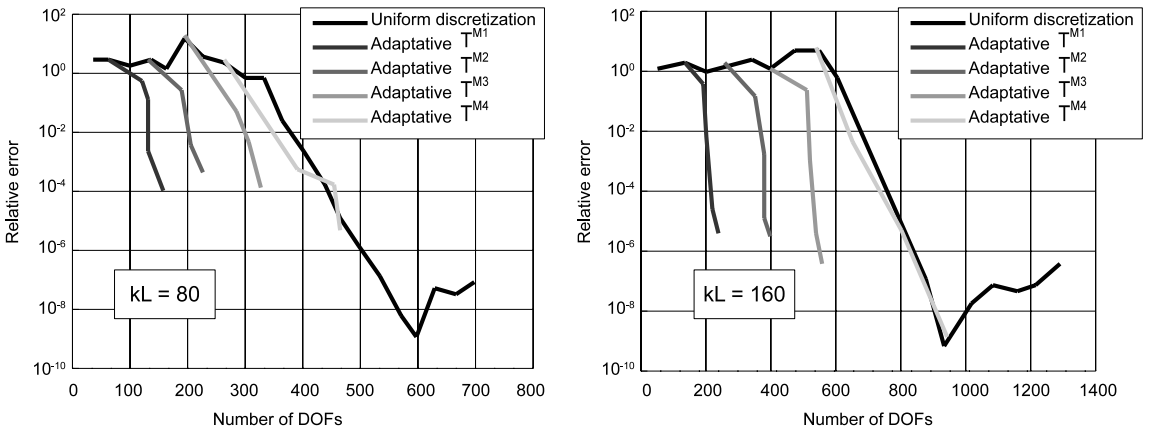


Fig. 10. The actual relative error of the adaptive VTCR in $\Omega$ as a function of the number of DOFs, and comparison with the nonadaptive VTCR (uniform discretization) for the first adaptive example (see Sec. 5.1). $T^{M1} = 0.2$, $T^{M2} = 0.4, T^{M3} = 0.6$, $T^{M4} = 0.8$ (see Fig. 9).

### 5.2. *Numerical results of an example based on a continuous distribution of propagative waves*

Now let us go back to the second numerical example of Sec. 3.3: A square acoustic cavity of width $L(\rho_0 = 1,3\,\mathrm{kg}\cdot\mathrm{m}^{-3}$ and $c_0 = 330\,\mathrm{m}\cdot\mathrm{s}^{-1})$ subjected along all four sides to a Robin condition with $Z = \rho_0 c_0$ and a prescribed excitation $h_d$ such that the exact wave amplitude is $A_{\mathrm{ex}}(\theta) = (1+i)\sin(4\theta)$ if $\theta \in ]-\pi/4;\pi/2[$, and $A_{\mathrm{ex}}(\theta) = 0$ otherwise. Two circular frequencies such that $kL = 80$ and $kL = 160$ were considered. Figure 6 shows the exact solution of this second numerical example with $kL = 80$. Again, we solved this problem using the VTCR with a uniform decomposition of $\Omega$ into $9 = 3 \times 3$ square subcavities.

As mentioned previously, this example is interesting because in the exact solution it involves a continuous distribution of propagative waves rather than some specific discrete propagation directions. Furthermore, the angular shape of the exact solution is sufficiently irregular to show how the adaptive method behaves in the case of rapidly oscillating representations.

We tested four values of parameter $T^M$: $T^{M1} = 0.2$, $T^{M2} = 0.4$, $T^{M3} = 0.6$ and $T^{M4} = 0.8$. A very large $T^m$ was used in order to evaluate the performance of the adaptive VTCR (see Fig. 11).

Figure 12 shows the adaptive solution obtained with $kL = 160$ at convergence. The angular distribution of the waves shows that the amplitudes of the waves are greatly influenced by the origin of the spatial coordinates, in this case the center of Cavity $\Omega_1$ (see the vector $\mathbf{x}_0$ in Fig. 6). Indeed, the phase of the solution changes drastically far away from the origin. In Cavity $\Omega_1$, however, the numerical solution obtained matches the exact solution perfectly.

Figure 13 shows the convergence curves as functions of the numbers of DOFs used compared with the nonadaptive VTCR with a uniform angular wave discretization. One can

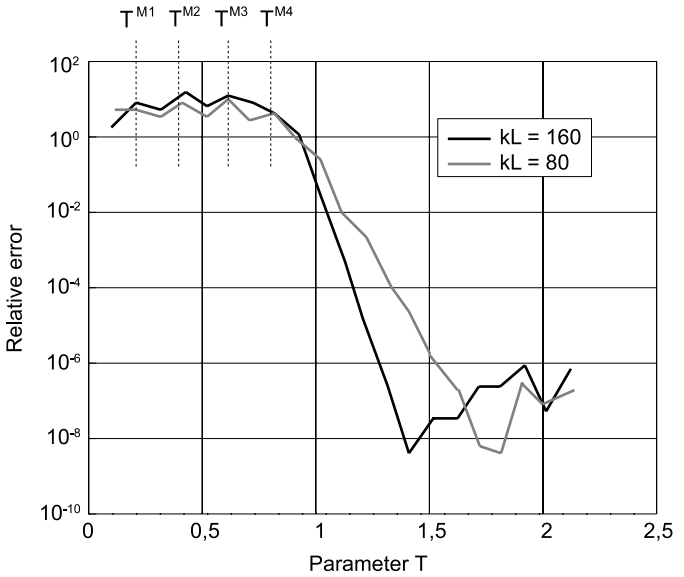


Fig. 11. The relative error in $L^2$ norm as a function of parameter $T$ (20) in subcavity $\Omega_5$ (see Fig. 6) for the second adaptive example (see Sec. 5.2).

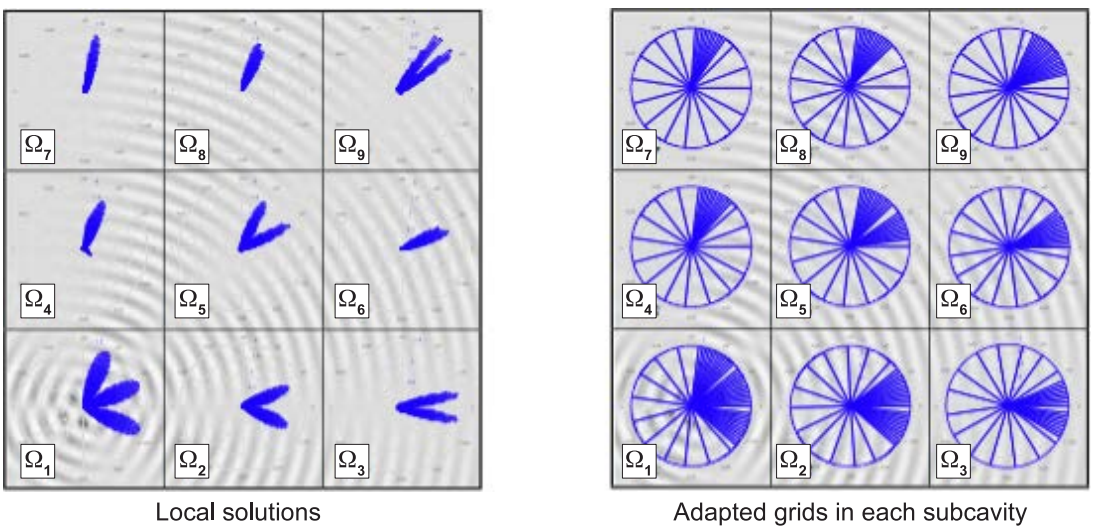


Fig. 12. The numerical solution for the second adaptive example (see Sec. 5.2) with $kL = 160$: (left) the angular wave distributions obtained in the various subcavities; (right) the angular distributions used in the various subcavities.

observe that the coarse grid greatly influences the quality of the solution. The more refined this grid, the better the solution. If parameter $\tau^M$ is too large, the strategy is no longer efficient. In that case, the error due to the coarse grid is greater than that due to the refined grid. In this situation, it would be more beneficial to increase $T^M$ than to increase $T^m$.

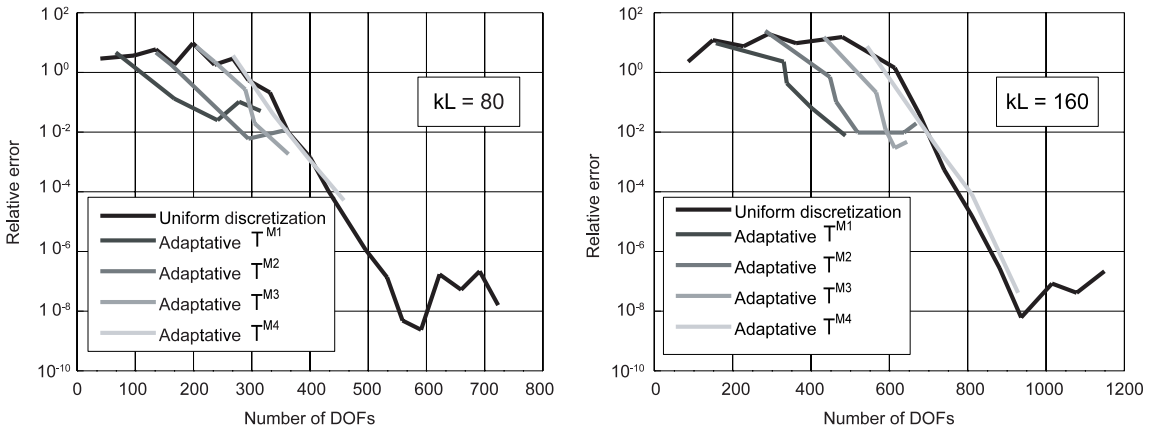


Fig. 13. The actual relative error of the adaptive VTCR as a function of the number of DOFs, and comparison with the nonadaptive VTCR (uniform discretization) for the second adaptive example (see Sec. 5.2). $T^{M1} = 0.2$, $T^{M2} = 0.4$, $T^{M3} = 0.6$, $T^{M4} = 0.8$ (see Fig. 11).

Of course, one can easily imagine that the procedure described previously is interesting only when the waves follow specific directions of propagation. Otherwise, a regular angular distribution of the waves is preferable. This is what the proposed strategy tends to do in such a case.

## 6. Conclusion

This paper discusses a new development of the VTCR for the study of interior steady-state dynamic problems governed by a Helmholtz-type partial differential equation. The objective is to improve the efficiency of the numerical handling of propagative waves in the case of highly directional solutions. In order to do that, we introduced an error indicator based on the consistency of the boundary conditions calculated in a subcavity. Then, we developed an adaptive wave approach which consists of three steps. In the first step, a calculation is performed with a coarse regular angular wave discretization, leading to a first approximation of the solution. In the second step, the angular errors are estimated using the error indicator and the angular zones where the wave discretization needs to be densified are determined. The third step consists in a new calculation with only a few waves in the directions in which few waves are needed, but many waves where the solution is highly directional. In order to do that, an energy-based angular error indicator was introduced to localize the angular directions where further refinement is needed. The methodology is presented in such a way that it can be applied to a general Helmholtz problem.

This strategy was applied successfully to two numerical examples of different complexity (a highly directional example and a more regular example). These examples prove the effectiveness of the error indicator and the capability of the proposed adaptive strategy to handle the different solutions: Using the error indicator we proposed, the angular directions which require further refinement could be determined; thanks to this refinement being limited to

the necessary directions alone, it was possible to calculate the vibrational behavior of the closed acoustic cavity efficiently. Both examples show the advantages of angular adaptivity in terms of convergence. Of course, the strategy also lends itself to the analysis of problems in which the angular discretization is completely regular.

The examples given showed that this strategy works at least for problems with between 13 and 25 wavelengths in the characteristic dimension of the problem. In particular, they showed that for a problem with a highly directional wave distribution, the adaptive strategy is very efficient and the coarse angular wave discretization can be chosen to be arbitrarily coarse. Predictably, however, for examples with continuous wave distributions, the adaptive strategy is less interesting and the coarse angular wave discretization must be refined in order to improve the accuracy.

Some subjects for future investigations are the extension of this adaptivity strategy to plate applications (for which edge waves exist) and the extension of the VTCR to 3D problems.

## References


1. O. C. Zienkiewicz, *The Finite Element Method* (McGraw-Hill, London, 1977).
2. C. A. Brebbia, *The Boundary Element Method for Engineers* (Pentech Press, London, 1978).
3. A. Deraemaeker, I. Babuska and P. Bouillard, Dispersion and pollution of the FEM solution for the Helmholtz equation in one, two and three dimensions, *Int. J. Numer. Met. Eng.* **46** (1999) 471–499.
4. R. Freymann, *Advanced Numerical and Experimental Methods in the Field of Vehicle Structural-Acoustics* (Hieronymus Buchreproduktions GmbH, München, 2000).
5. C. Soize, Reduced models in the medium frequency range for the general dissipative structural dynamic systems, *Eur. J. Mech. Solid.* **17** (1998) 657–685.
6. I. Harari and T. J. R. Hughes, Galerkin/least-squares finite element methods for the reduced wave equation with non-reflecting boundary conditions in unbounded domains, *Comput. Met. Appl. Mech. Eng.* **98**(3) (1992) 411–454.
7. I. Babuska, F. Ihlenburg, E. T. Paik and S. A. Sauter, A generalized finite element method for solving the helmholtz equation in two dimensions with minimal pollution, *Comput. Met. Appl. Mech. Eng.* **128** (1995) 325–359.
8. J. M. Melenk and I. Babuska, The partition of unity finite element method: Basic theory and applications, *Comput. Met. Appl. Mech. Eng.* **139** (1996) 289–314.
9. J. M. Melenk and I. Babuska, Approximation with harmonic and generalized harmonic polynomials in the partition of unity method, *Comput. Assist. Mech. Eng. Sci.* **4** (1997) 607–632.
10. T. Strouboulis, K. Copps and I. Babuska, The generalized finite element method: An example of its implementation and illustration of its performance, *Int. J. Numer. Met. Eng.* **47** (2000) 1401–1417.
11. T. J. R. Hughes, Multiscale phenomena: Greens functions and the dirichlet-to-neumann formulation and subgrid scale models and bubbles and the origins of stabilized methods, *Comput. Met. Appl. Mech. Eng.* **127** (1995) 387–401.
12. L. P. Franca, C. Farhat, A. P. Macedo and M. Lesoinne, Residual-free bubbles for the helmholtz equation, *Int. J. Numer. Met. Eng.* **40** (1997) 4003–4009.

13. L. F. Greengard and V. Rokhlin, A fast algorithm for particle simulations, *J. Comput. Phys.* **73** (1987) 325–348.
14. M. Bonnet, S. Chaillat and J.-F. Semblat, A multi-level fast multipole BEM for 3-D elastodynamics in the frequency domain, *Comput. Met. Appl. Mech. Eng.* **197** (2008) 4233–4249.
15. E. de Langre, Fonctions de transfert de plaques par équations intégrales. Test de validation et de performance, Rapport CEA: DMT/90/395 (1991) (in French).
16. I. Harari and T. J. R. Hugues, A cost comparison of boundary element and finite element methods for problems of time-harmonic acoustics, *Comput. Met. Appl. Mech. Eng.* **97** (1992) 77–102.
17. E. Trefftz, Ein gegenstuck zum ritzschen verfahren, in *Second International Congress on Applied Mechanics* (1926), pp. 131–137 (in German).
18. O. Laghrouche and P. Bettess, Short wave modelling using special finite elements, *J. Comput. Acoust.* **8** (2000) 189–210.
19. T. Strouboulis, I. Babuska and R. Hidajat, The generalized finite element method for helmholtz equation: Theory and computation and and open problems, *Comput. Met. Appl. Mech. Eng.* **195** (2006) 4711–4731.
20. T. Strouboulis and R. Hidajat, Partition of unity method for helmholtz equation: q-convergence for plane-wave and wave-band local bases, *Appl. Math.* **51** (2006) 181–204.
21. O. Cessenat and B. Despres, Application of an ultra weak variational formulation of elliptic pdes to the two-dimensional helmholtz problem, *SIAM J. Numr. Anal.* **35** (1998) 255–299.
22. P. Monk and D. Q. Wang, A least-squares method for the helmholtz equation, *Comput. Met. Appl. Mech. Eng.* **175** (1999) 121–136.
23. C. Farhat, I. Harari and L. P. Franca, The discontinuous enrichment method, *Comput. Met. Appl. Mech. Eng.* **190** (2001) 6455–6479.
24. P. Bouillard and S. Suleau, Element-free galerkin solutions for helmholtz problems: Formulation and numerical assessment of the pollution effect, *Comput. Met. Appl. Mech. Eng.* **162** (1998) 317–335.
25. E. Perrey-Debain, J. Trevelyan and P. Bettess, Wave boundary elements: A theoretical overview presenting applications in scattering of short waves, *Eng. Anal. Boundary Elem.* **28** (2004) 131–141.
26. W. Desmet, P. Sas and D. Vandepitte, An indirect trefftz method for the steady-state dynamic analysis of coupled vibro-acoustic systems, *Comput. Assist Mech. Eng. Sci.* **8** (2001) 271–288.
27. P. Ladevèze, A new computational approach for structure vibrations in the medium frequency range, *Comptes Rendus Académie des Sciences Paris* **322(IIb)** (1996) 849–856 (in French).
28. P. Ladevèze, L. Arnaud, P. Rouch and C. Blanzé, The variational theory of complex rays for the calculation of medium-frequency vibrations, *Eng. Comput.* **18** (2001) 193–214.
29. R. Rouch and P. Ladevèze, The variational theory of complex rays: A predictive tool for medium-frequency vibrations, *Comput. Met. Appl. Mech. Eng.* **192** (2003) 3301–3315.
30. P. Ladevèze, L. Blanc, P. Rouch and C. Blanzé, A multiscale computational method for medium-frequency vibrations of assemblies of heterogeneous plates, *Comput. Struct.* **81** (2003) 1267–1276.
31. H. Riou, P. Ladevèze and P. Rouch, Extension of the variational theory of complex rays to shells for medium-frequency vibrations, *J. Sound Vib.* **272** (2004) 341–360.
32. P. Ladevèze, P. Rouch, H. Riou and X. Bohineust, Analysis of medium-frequency vibrations in a frequency range, *J. Comput. Acoust.* **11** (2003) 255–284.
33. P. Ladevèze and M. Chevreuil, A new computational method for transient dynamics including the low- and the medium-frequency ranges, *Int. J. Numer. Met. Eng.* **64** (2005) 503–527.
34. H. Riou, P. P. Ladevèze and B. Sourcis, The multiscale VTCR approach applied to acoustics problems, *J. Comput. Acoust.* **16** (2008) 487–505.

35. B. Sourcis, Toward an adaptative strategy for the variational theory of complex rays: Application to linear acoustic, PhD thesis (2009).
36. J. M. Melenk, On generalized finite element method, PhD thesis, University of Maryland (1995).
37. R. S. James and T. J. R. Hughes, h-Adaptive finite element computation of time-harmonic exterior acoustics problems in two dimensions, *Comput. Met. Appl. Mech. Eng.* **146** (1997) 65–89.